Physical Modeling of Vibrating Plates

Maximilian Schäfer, Manuel Werner and Rudolf Rabenstein
Multimedia Communications and Signal Processing (LMS)
Friedrich-Alexander-Universität Erlangen-Nürnberg (FAU)
Cauerstr.7, 91058 Erlangen, Germany
Email: max.schaefer@fau.de, rudolf.rabenstein@fau.de

Introduction

The application of physical modeling techniques allows the derivation of powerful and efficient simulation models of physical systems in the discrete time domain, which can be used in real-time musical applications [1, 2]. The modeling of membranes and vibrating plates including non-linear and anisotropic plates is discussed in [1, 3–9] and the modeling of guitar and piano strings in [10, 11]. The incorporation of realistic coupling and boundary conditions for systems based on physical models is discussed in [12–14].

Many percussive instruments as drumheads or xylophones and also reverberation plates are physically based on Kirchhoff's thin plate equation. The behaviour of such systems can be described by a partial differential equation for the plate deflection. It is completed by a suitable set of initial and boundary conditions to constitute an initial-boundary value problem [15]. An appropriate modeling technique for systems described by initial-boundary value problems is based on functional transformations, where a linear spatial differential operator is expanded into a set of bi-orthogonal eigenfunctions [16,17]. The corresponding eigenvalues characterize the oscillation modes of the system. They can be derived in a closed form for Dirichlet boundary conditions. The eigenfunction expansion has been formulated either as a multidimensional state-space description, which provides a powerful analytical form [14, 18] or as a parallel structure of 2nd order filters to achieve an efficient real-time algorithm [8].

This contribution derives a simulation model for the deflection of a thin rectangular plate by the application of functional transformations. The starting point is Kirchhoff's thin plate equation, which is extended by several damping terms to introduce damping and dispersion into the system, where the influence of these terms is discussed from a system theoretic viewpoint. In the end a discrete time simulation algorithm is derived, which is used for simulations of the plate deflection.

The paper is structured as follows: First, the physical foundations of the damped thin plate equation are presented and the applied functional transformations are introduced, which are used to derive a simulation model. Then the influence of frequency independent and depending damping is discussed and simulation results for the plate deflection are shown. Finally, the paper is concluded and topics for further works are addressed.

Physical Description

Fig. 1 depicts the geometry of a rectangular plate, which is determined by its lengths L_x, L_y and height h. The height h is a assumed to be small, i.e. $h \ll L_x, L_y$. The vibration of such a plate is described by Kirchhoff's thin plate equation [19] in terms of its space- and time-dependent deflection $w(x, y, t)$ in z-direction.

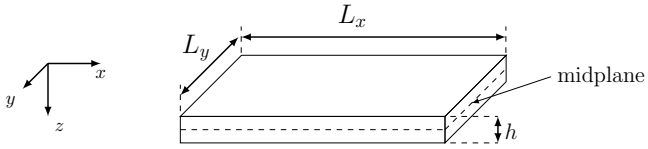

Figure 1: Three-dimensional thin plate with the lengths L_x, L_y and the height h.

The classical form of this partial differential equation (PDE) does not contain any damping. However, for the purpose of sound synthesis and to arrive at realistic sounding models, several valid extensions have been applied to the classical thin plate equation [5]. These extensions introduce frequency dependent and independent damping into the plate description [7, 9]

$$\begin{aligned}\boldsymbol{\Delta\Delta} w(x,y,t) + R \cdot \partial_{tt} w(x,y,t) + d_1 \cdot \partial_t w(x,y,t) \\ -d_3 \cdot \partial_t \boldsymbol{\Delta} w(x,y,t) = f_\mathrm{e}(x,y,t),\end{aligned} \tag{1}$$

with the bi-harmonic operator $\boldsymbol{\Delta\Delta} = (\partial_{xx} + \partial_{yy})^2$ and $R = \frac{\rho h}{D}$. The operators ∂_x, ∂_y are partial derivatives in x-direction and in y-direction. Additional damping is represented by the coefficients $d_1 = {}^{d_\mathrm{i}}/_{D}$, $d_3 = {}^{d_\mathrm{f}}/_{D}$ including the damping terms d_i and d_f for frequency independent and frequency dependent damping, respectively. The constant D defines the flexural rigidity $D = \frac{Eh^3}{12(1-\nu^2)}$ in terms of Young's modulus E and the Poisson number ν.

At the system boundaries it is assumed that the plate is simply supported, which can be formulated as a set of Dirichlet boundary conditions defined at the boundaries of the plate $x = 0, L_x$ and $y = 0, L_y$ [1, 19]

$$w(x,y,t) = 0, \quad m^{(x)}(x,y,t) = 0, \quad m^{(y)}(x,y,t) = 0. \tag{2}$$

As the temporal initial state of the plate it is assumed, that the plate is at rest for $t = 0$. This constitutes the initial condition $w(x, y, t = 0) = 0$.

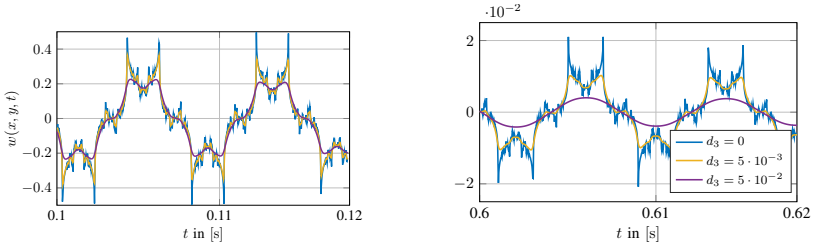

Figure 2: Temporal progression of the deflection $w(\boldsymbol{x}, t)$ on the plate for different frequency dependent damping ($d3$) shortly after the excitation (left) and in the release phase (right)

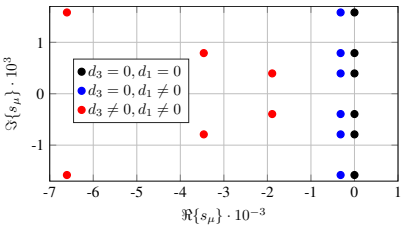

Figure 3: Pole-zero plot of the plate for three different damping scenarios.

Vector Formulation

For the application of the functional transformations and to obtain a higher variety of physical quantities in the solution, it is of advantage to reformulate Eq. (1) in terms of the vector of variables

$$\boldsymbol{y}(x,y,t) = \begin{bmatrix} w(x,y,t) \\ v(x,y,t) \\ m^{(x)}(x,y,t) \\ m^{(y)}(x,y,t) \\ m^{(xy)}(x,y,t) \end{bmatrix}, \tag{3}$$

containing the deflection w, the velocity $v = \partial_t w$ as well as the moments $m^{(x)}$ and $m^{(y)}$ in x- and y-direction, respectively, and the mixed moment $m^{(xy)}$. This reformulation into a vector form leads to a unified vector formulation of the PDE (1) in the region $0 \leq x \leq L_x$, $0 \leq y \leq L_y$ and with $\boldsymbol{x} = [x, y]^{\mathrm{T}}$ [20]

$$[\partial_t \boldsymbol{C} - \boldsymbol{L}]\, \boldsymbol{y}(\boldsymbol{x}, t) = \boldsymbol{f}_{\mathrm{e}}(\boldsymbol{x}, t), \qquad \boldsymbol{L} = \boldsymbol{A} + \boldsymbol{\nabla B}. \tag{4}$$

The matrix $\boldsymbol{C}$ is a capacitance matrix and the matrix $\boldsymbol{A}$ contains the damping parameters. The spatial derivatives in (1) are merged into the spatial differential operator $\boldsymbol{L}$, so that the product $\boldsymbol{\nabla B y}$ resembles the biharmonic operator in (1). The exact structures of the matrices $\boldsymbol{A}, \boldsymbol{C}, \boldsymbol{\nabla B}$ are not shown in this contribution for brevity, but they can be easily calculated by the reformulation of (1) into (4) with the vector (3).

Laplace Transformation

The application of a one-sided Laplace transform to the vector PDE (1) leads to a representation in the continuous frequency domain

$$[s\boldsymbol{C} - \boldsymbol{L}]\, \boldsymbol{Y}(\boldsymbol{x}, s) = \boldsymbol{F}_{\mathrm{e}}(\boldsymbol{x}, s). \tag{5}$$

Upper case letters denote variables and vectors in the continuous frequency domain and s is the complex frequency variable.

The Laplace transformation removes the time derivative in the PDE (4) and replaces it by a multiplication with the complex frequency variable s, see (5). It would correctly consider also any non-zero initial conditions. This feature is not required here.

Functional Transformations

The solution of the PDE (5) in the frequency domain is expanded into an infinite set of bi-orthogonal eigenfunctions $\boldsymbol{K}, \tilde{\boldsymbol{K}}$, with the dedicated eigenvalues s_μ. The eigenfunctions and eigenvalues describe the oscillation modes of the plate [17]. The expansion leads to a representation in terms of multidimensional transfer functions in a spatio-temporal transform domain, formulated in a state-space description [14, 18]. For the expansion of (5) a pair of forward and inverse functional transformations can be defined.

The forward transformation is performed by a set of adjoint eigenfunctions $\tilde{\boldsymbol{K}}$ arranged in the matrix $\tilde{\boldsymbol{\mathcal{C}}}$ to convert the vector of variables from (3) into its spatial transform domain version $\bar{\boldsymbol{Y}}$ [21]

$$\boldsymbol{\mathcal{T}}\{\boldsymbol{Y}(\boldsymbol{x}, s)\} = \bar{\boldsymbol{Y}}(s) = \left\langle \boldsymbol{C}\boldsymbol{Y}(\boldsymbol{x}, s), \tilde{\boldsymbol{\mathcal{C}}}(\boldsymbol{x}) \right\rangle. \tag{6}$$

The scalar product $\langle\, , \rangle$ is defined as a two-dimensional integration over the spatial extension of the plate.

Analogously, the inverse transformation applies a set of primal eigenfunctions $\boldsymbol{K}$ arranged in the matrix $\boldsymbol{\mathcal{C}}$ to the transform domain representation $\bar{\boldsymbol{Y}}$. It can also be formulated in a more straightforward way as a sum over all possible modes of the plate

$$\begin{aligned} \boldsymbol{\mathcal{T}}^{-1}\{\bar{\boldsymbol{Y}}(s)\} &= \boldsymbol{Y}(\boldsymbol{x}, s) \\ &= \sum_{\mu=0}^{\infty} \frac{1}{N_\mu} \bar{Y}(\mu, s) \boldsymbol{K}(\boldsymbol{x}, \mu) = \boldsymbol{\mathcal{C}}(x) \bar{\boldsymbol{Y}}(s). \end{aligned} \tag{7}$$

Applying the forward transformation (6) to the vector PDE (5), leads to a representation of the PDE in the spatio-temporal transform domain

$$s\bar{\boldsymbol{Y}}(s) = \boldsymbol{\mathcal{A}}\bar{\boldsymbol{Y}}(s) + \bar{\boldsymbol{\Phi}}(s) + \bar{\boldsymbol{F}}_{\mathrm{e}}(s), \tag{8}$$

where $\bar{\boldsymbol{F}}_{\mathrm{e}}$ is the transform domain representation of the excitation function. The influence of the boundary conditions constitutes the vector $\bar{\boldsymbol{\Phi}}$ containing the transformed boundary values. For the given scenario of simply supported edges (see (2)), the boundary term vanishes, so that $\bar{\boldsymbol{\Phi}} = \boldsymbol{0}$.

Together, Eq. (8), (7) constitute a state-space description. The state equation (8) is in the spatio-temporal transform domain (dynamics of $\bar{\boldsymbol{Y}}$) and the output equation (7) transforms the system back into the space domain ($\bar{\boldsymbol{Y}} \rightarrow \boldsymbol{Y}$).

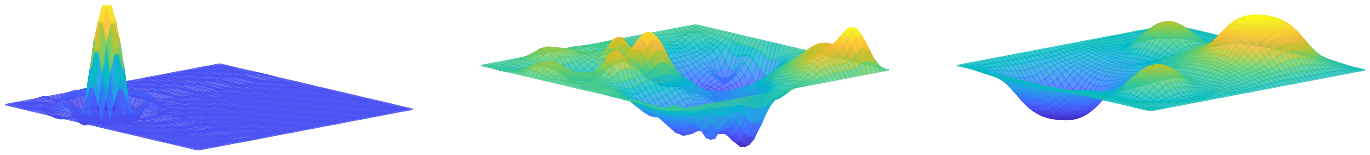

Figure 4: Spatial distribution of the deflection $w(x, y, t)$ at $t = 0$ while the excitation by a single impulse (left), $t = 0.1$s shortly after the excitation (mid) and in the release phase $t = 0.6$s (right)

Eigenfunctions and Eigenvalues

The eigenfunctions $\boldsymbol{K}$, $\tilde{\boldsymbol{K}}$ are derived from their dedicated eigenvalue problems [14, 20]

$$\boldsymbol{L}\boldsymbol{K} = s_\mu \boldsymbol{C}\boldsymbol{K}, \tag{9}$$

$$\tilde{\boldsymbol{L}}\tilde{\boldsymbol{K}} = s_\mu^* \boldsymbol{C}^{\mathrm{H}}\tilde{\boldsymbol{K}}, \tag{10}$$

where $\tilde{\boldsymbol{L}}$ is the adjoint spatial differential operator to $\boldsymbol{L}$. The calculation of the eigenfunctions $\boldsymbol{K}$ and $\tilde{\boldsymbol{K}}$ has to consider the boundary conditions and is not discussed in this contribution for brevity. The solution of (9), (10) yields also the dispersion relation (see (12)) and the eigenvalues s_μ. A detailed description, how these eigenvalue problems are solved and how the eigenfunctions and eigenvalues can be calculated is given in [14, 17, 22].

Simulation Algorithm

For the derivation of a discrete time simulation algorithm, the state equation (8) and the output equation (7) are transformed into the discrete time domain by the impulse-invariant transformation

$$\bar{\boldsymbol{y}}[k] = e^{\boldsymbol{\mathcal{A}}\cdot T}\bar{\boldsymbol{y}}[k-1] + \bar{\boldsymbol{f}}_{\mathrm{e}}[k], \quad \boldsymbol{y}[\boldsymbol{x}, k] = \boldsymbol{\mathcal{C}}(\boldsymbol{x})\bar{\boldsymbol{y}}[k], \tag{11}$$

where k is the discrete time variable with $t = kT$ and the sampling rate $f_{\mathrm{s}} = 1/T$. For practical simulations, the infinite number of eigenvalues in (11) is restricted to a finite number of M and therefore $\mu = 0, \ldots, M-1$. The matrix exponential $e^{\boldsymbol{\mathcal{A}}\cdot T}$ is evaluated by methods described e.g. in [22].

Damping and Dispersion

The different damping terms d_1, d_3 in (1) determine the sound of the plate model in different ways. To get a feeling on how these terms influence the oscillations of a plate, the dispersion relation

$$R \cdot s_\mu^2 + \left(d_1 + d_3\left(\lambda_x^2 + \lambda_y^2\right)\right) \cdot s_\mu + \left(\lambda_x^2 + \lambda_y^2\right)^2 = 0, \tag{12}$$

and the eigenvalues derived thereof are inspected. The real and imaginary parts σ and ω of the eigenvalues follow as

$$s_\mu = \sigma(\lambda_x, \lambda_y) \pm \mathrm{j}\omega(\lambda_x, \lambda_y), \tag{13}$$

$$\sigma(\lambda_x, \lambda_y) = -\frac{1}{2R}\left(d_1 + d_3\left(\lambda_x^2 + \lambda_y^2\right)\right), \tag{14}$$

$$\omega(\lambda_x, \lambda_y) = \frac{1}{2R}\sqrt{4R\left(\lambda_x^2 + \lambda_y^2\right)^2 - \left(d_1 + d_3\left(\lambda_x^2 + \lambda_y^2\right)\right)}. \tag{15}$$

The frequency independent term d_1 introduces natural damping by e.g. friction into the system. As it can be seen in (14) and (15), its influence is not multiplied by the individual wavenumbers λ_x, λ_y in x- and y-direction, respectively. This leads to a uniform damping for all oscillation modes. The term d_3 introduces frequency dependent damping into the system, as can also be seen in (14) and (15), where the amount of damping by d_3 scales with the wave numbers. This effect ensures, that higher frequency oscillations attenuate faster than the low frequency oscillations. The same effects can also be observed in Figs. 2 and 3. Figure 2 shows the impulse response of the plate calculated with (11) after the excitation (left) and in the release phase (right) for three different values of d_3. The figure reflects the effects inspected in (10): the larger d_3, the faster decays the high frequency content. The influence of both damping terms on the eigenvalues is shown graphically in the s-plane in Fig. 3. For further reading about the different kinds of damping of plates, see [5, 6, 23].

Simulation Results

The following section presents the simulation results for the deflection of an oscillating thin plate. All simulations are conducted with the discrete time simulation model in (11) and a sampling frequency of $f_{\mathrm{s}} = 44.1$kHz. The plate is defined by its parameters as: $L_x = L_y = 0.2\,\mathrm{m}$, $h = 1\,\mathrm{mm}$, $\rho = 7850\,\mathrm{kg/m^2}$, $E = 220\,\mathrm{GPa}$, $\nu = 0.3$. The dimensions of the damping parameters are chosen according to [7] as: $d_{\mathrm{i}} = 1 \cdot 10^2\,\mathrm{kg/m^2 s}$, $d_{\mathrm{f}} = 5 \cdot 10^{-4}\,\mathrm{kg\,s^{-1}}$. For all simulations a total number of $M = 400$ complex conjugate pairs of eigenvalues was used. The plate is excited by a delta-impulse in time and space $f_{\mathrm{e}}(\boldsymbol{x}_{\mathrm{e}}, t) = \delta(t) \cdot \delta(x - x_{\mathrm{e}})\delta(y - y_{\mathrm{e}})$ at $\boldsymbol{x}_{\mathrm{e}} = [\frac{1}{4}L_x,\ \frac{1}{4}L_y]$. The single impulse is suitable for an analysis in a system theoretic sense, but it has to deal with discontinuities and therefore with Gibb's phenomenon. For the preparation of realistic sound examples, or the usage in a musical context, the excitation function has to be chosen to be a smoother function, e.g. a raised-cosine function [10].

Figure 4 shows the spatial distribution of the deflection w on the plate for three different temporal positions and resembles the results in Fig. 2. The left figure shows the plate at the time of excitation ($t = 0$), where the impulse is clearly visible. The center plot shows the plate deflection shortly after the excitation $t = 0.1$s and justifies the left plot in Fig. 2. At this temporal position, the oscillation of the plate is very rich in high frequency content. Finally, the right plot shows the plate in the decay phase

($t = 0.6$s) and it corresponds to the right plot in Fig. 2. Most of the high frequency content is attenuated by the influence of d_3 and only low frequency oscillations are left.

Conclusions

In this contribution a discrete time simulation model for an isotropic thin plate was derived and formulated in terms of a state-space description. The additional damping terms in Kirchhoff's thin plate equation have been analysed w.r.t. their influence on the eigenvalues and the impulse response of the plate. The validity of the derived algorithm has been shown by the simulation of the spatial distribution of the plate deflection.

The following topics are addressed for further works: Incorporation of complex boundary conditions by a feedback loop structure from control theory [9], extension of the model to non-linear and anisotropic plates [1, 3], comparisons to plate measurements and the design of a framework for player interconnection.

References

[1] S. Bilbao, *Numerical Sound Synthesis*. Chichester, UK: John Wiley and Sons, 2009.

[2] J. Bensa, S. Bilbao, R. Kronland-Martinet, and J. O. Smith, "The simulation of piano string vibration: From physical models to finite difference schemes and digital waveguides," *J. Acoustical Society of America*, vol. 114, no. 2, pp. 1095–1107, 2003. [Online]. Available: http://scitation.aip.org/content/asa/journal/jasa/114/2/10.1121/1.1587146

[3] S. Bilbao, "Sound Synthesis for Nonlinear Plates," in *8th Int. Conf. Digital Audio Effects (DAFx-05)*, Madrid, 9 2008, pp. 243–248.

[4] S. Bilbao and M. van Walstijn, "A finite difference plate model," in *ICMC*, 2005.

[5] A. Chaigne and C. Lambourg, "Time-Domain Simulation of Damped Impacted Plates. I. Theory and Experiments," *The Journal of the Acoustical Society of America*, vol. 109, no. 4, pp. 1422–1432, 2001. [Online]. Available: https://asa.scitation.org/doi/abs/10.1121/1.1354200

[6] C. Lambourg, A. Chaigne, and D. Matignon, "Time-Domain Simulation of Damped Impacted Plates. II. Numerical Model and Results," *The Journal of the Acoustical Society of America*, vol. 109, no. 4, pp. 1433–1447, 2001. [Online]. Available: https://asa.scitation.org/doi/abs/10.1121/1.1354201

[7] F. Avanzini and R. Marogna, "A Modular Physically Based Approach to the Sound Synthesis of Membrane Percussion Instruments," *IEEE Transactions on Audio, Speech, and Language Processing*, vol. 18, no. 4, pp. 891–902, May 2010.

[8] R. Rabenstein, T. Koch, and C. Popp, "Tubular Bells: A Physical and Algorithmic Model," *IEEE Transactions on Audio, Speech, and Language Processing*, vol. 18, no. 4, pp. 881–890, 2010.

[9] M. Schäfer, M. Werner, and R. Rabenstein, "Physical Modeling in Sound Synthesis: Vibrating Plates," in *26th International Congress on Sound and Vibration (ICSV26)*, Montreal, Canada, 2019, accepted for publication.

[10] M. Schäfer, P. Frenstátský, and R. Rabenstein, "A physical string model with adjustable boundary conditions," in *19th International Conference on Digital Audio Effects (DAFx-16)*, Brno, Czech Republic, Sep 2016, pp. 159 – 166. [Online]. Available: http://dafx16.vutbr.cz/

[11] R. Rabenstein and L. Trautmann, "Digital Sound Synthesis of String Instruments with the Functional Transformation Method," *Signal Processing*, vol. 83, no. 8, pp. 1673–1688, August 2003.

[12] M. Van Walstijn and S. Mehes, "An Explorative String-Bridge-Plate Model with Tunable Parameters," in *Proceedings of the 20th International Conference on Digital Audio Effects (DAFx-17)*, Edinburgh, 2017, pp. 291–298.

[13] M. Schäfer and R. Rabenstein, "A Continuous Frequency Domain Description of Adjustable Boundary Conditions for Multidimensional Transfer Function Models," in *20th International Conference on Digital Audio Effects (DAFx-17)*, Edinburgh, 2017.

[14] R. Rabenstein, M. Schäfer, and C. Strobl, "Transfer Function Models for Distributed-Parameter Systems with Impedance Boundary Conditions," *International Journal of Control*, vol. 91, no. 12, pp. 2726–2742, 2018. [Online]. Available: https://doi.org/10.1080/00207179.2017.1397753

[15] N. H. Fletcher and T. D. Rossing, *The Physics of Musical Instruments*, 2nd ed. New York, USA: Springer-Verlag, 1998.

[16] H. Zwart, "Transfer functions for infinite-dimensional systems," *Systems & Control Letters*, vol. 52, no. 3, pp. 247 – 255, 2004. [Online]. Available: http://www.sciencedirect.com/science/article/pii/S016769110400009X

[17] R. V. Churchill, *Operational Mathematics*. Boston, Massachusetts: Mc Graw Hill, 1972.

[18] J. Deutscher and C. Harkort, "Parametric State Feedback Design of Linear Distributed-Parameter Systems," *International Journal of Control*, vol. 82, no. 6, pp. 1060–1069, 2009. [Online]. Available: http://www.tandfonline.com/doi/abs/10.1080/00207170802434383

[19] P. L. Gould, *Analysis of Shells and Plates*. Springer-Verlag New York, 1988.

[20] S. Petrausch and R. Rabenstein, "A Simplified Design of Multidimensional Transfer Function Models," in *International Workshop on Spectral Methods and Multirate Signal Processing (SMMSP2004)*, Vienna, Austria, September 2004, pp. 35–40.

[21] M. Schäfer, W. Wicke, R. Rabenstein, and R. Schober, "An nD Model for a Cylindrical Diffusion-Advection Problem with an Orthogonal Force Component," in *23rd International Conference on Digital Signal Processing (DSP 2018)*, Shanghai, 2018.

[22] M. Schäfer and R. Rabenstein, "Calculation of the Transformation Kernels for the Functional Transformation Method," in *10th International Workshop on Multidimensional (nD) Systems (nDS 2017)*, Zielona Góra, 2017.

[23] N. H. Fletcher and T. D. Rossing, *Principles of Vibration and Sound*. New York, USA: Springer-Verlag, 1995.